

In-Situ Manipulation of the Magnetic Anisotropy of Single Mn Atom via Molecular Ligands

Peng Cheng,[#] Longjuan Kong,[#] Tong Zhang,[#] Hang Liu, Huixia Fu, Lan Chen, Kehui Wu, Xi Chen, Sheng Meng, and Qi-kun Xue^{*}

Cite This: *Nano Lett.* 2021, 21, 3566–3572

Read Online

ACCESS |

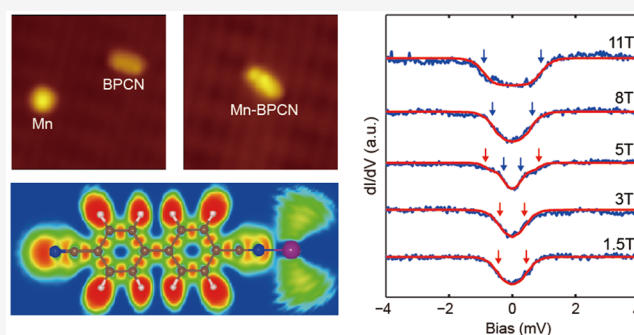
Metrics & More

Article Recommendations

Supporting Information

ABSTRACT: Magnetic anisotropy is essential for permanent magnets to maintain their magnetization along specific directions. Understanding and controlling the magnetic anisotropy on a single-molecule scale are challenging but of fundamental importance for the future's spintronic technology. Here, by using scanning tunneling microscopy (STM), we demonstrated the ability to control the magnetic anisotropy by tuning the ligand field at the single-molecule level. We constructed a molecular magnetic complex with a single Mn atom and an organic molecule (4,4'-biphenyldicarbonitrile) as a ligand via atomic manipulation. Inelastic tunneling spectra (IETS) show that the Mn complex has much larger axial magnetic anisotropy than individual Mn atoms, and the anisotropy energy can be tuned by the coupling strength of the ligand. With density functional theory calculations, we revealed that the enhanced magnetic anisotropy of Mn arising from the carbonitrile ligand provides a prototype for the engineering of the magnetism of quantum devices.

KEYWORDS: *Magnetic anisotropy, molecular ligands, spin-flip excitations, atomic manipulation*



Magnetic anisotropy plays a key role in permanent magnets to maintain their direction of magnetization over time.^{1,2} It is manifested as the tendency for the magnetization to align along specific directions despite thermal fluctuations. Magnetic anisotropy can also be evolved in magnetic structures with only a few atomic spins, such as single atoms and single molecules.^{3–5} The large anisotropies in these atomic scale structures enable them to exhibit intriguing quantum effects and also make them attractive for miniaturized data storage applications and quantum computing.^{6–8}

Recently, surface adsorption and structure distortion-induced^{9–15} or organic ligand-induced^{16–23} magnetic anisotropy of individual magnetic atoms/molecules have been reported. Whereas the exchange interaction of electrons spins is isotropic, the crystal field or the ligand field surrounding the magnetic atom could offer additional degrees of freedom to tune its spin and orbital and thus give rise to the magnetic anisotropy by spin–orbital coupling. Therefore, the surrounding environment of the magnetic atom could be utilized to manipulate the anisotropy of the single atom or single molecule, which is crucial for its potential applications.

In this work, by using low-temperature STM and atomic manipulation, we introduced significant magnetic anisotropy to a single Mn atom by bonding it to an organic ligand with a carbonitrile group. This single molecular chemical reaction was performed on ultrathin lead oxide (PbO) layers grown on Pb/

Si(111), which acts as a decoupling layer on the metal substrate. The magnetic properties of the resulting complex were probed by inelastic tunneling spectroscopy (IETS).^{24–26} Significant zero-field splitting in the IETS suggests a large in-plane magnetic anisotropy for the complex. In addition, the zero-field splitting energy of the Mn complex varies with the distance between the Mn atom and the ligand, implying that the anisotropy of the magnetic complex can further be tuned by the coupling strength of the ligand field. Our DFT calculations prove that the system has an in-plane magnetic polarization and the easy-axis lies perpendicular to the axial line of the ligand.

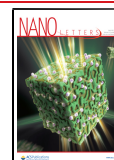
EXPERIMENTAL SECTION

The experiments were performed in an ultrahigh vacuum ³He cooling STM system at the base temperature of 0.4 K. A magnetic field up to 11 T can be applied perpendicular to the surface of the sample. All the tunneling spectra were recorded at 0.4 K by a lock-in technique with the feedback loop

Received: February 8, 2021

Revised: March 30, 2021

Published: April 8, 2021



switched off. A superconducting niobium tip was used to improve the energy resolution near the Fermi level.²⁷ The PbO layers were grown on Pb(111) film on Si(111) substrate by a two-step oxidation method²⁸ (see Figure S1(a) for a large-scale STM image of PbO/Pb/Si(111) film). The two-layer-thick insulating PbO will suppress the electron density of states around the Fermi level to increase the spin lifetime of magnetic adsorbates,²⁹ which is critical for the IETS measurement. Manganese atoms and organic ligands (4,4'-biphenyldicarbonitrile, BPCN) were deposited onto the PbO/Pb/Si(111) film at a temperature below 50 K. A large-scale STM image after Mn deposition is shown in Figure S1(b). The methods for first-principles calculations are included in the Supporting Information.

RESULTS AND DISCUSSION

Figure 1(a) shows a typical surface topography after Mn atoms were deposited on PbO/Pb/Si(111) films. Individual Mn atoms appear as identical round protrusions with an apparent height of 0.25 nm. The tunneling spectra (dI/dV) measured on a single Mn atom under various magnetic fields (perpendicular to the surface) are shown in Figure 1(b). They display two

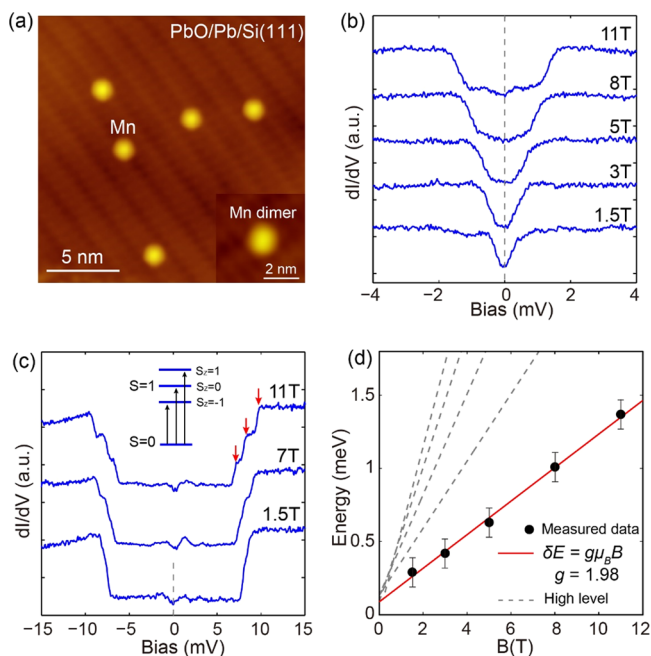


Figure 1. Mn atoms on PbO and their tunneling spectra. (a) STM image ($18.3 \times 18.3 \text{ nm}^2$, $V = 1.0 \text{ V}$, $I = 0.1 \text{ nA}$) of five individual Mn atoms adsorbed on a PbO island on Pb(111); the insert image ($5 \times 5 \text{ nm}^2$, $V = 1.0 \text{ V}$, $I = 0.1 \text{ nA}$) shows a Mn dimer constructed by atom manipulation. (b) dI/dV spectra of a single Mn atom taken at 0.4 K with magnetic field perpendicular to the surface. Tunneling junction: $V = 10 \text{ mV}$, $I = 0.4 \text{ nA}$. Bias modulation: $50 \mu\text{V}$, 991 Hz . (c) dI/dV spectra of the Mn dimer taken at 0.4 K with a magnetic field perpendicular to the surface, where the tunneling junction is the same as in (b). All the curves are offset vertically for clarity. The red arrows indicate three substeps at $B = 11 \text{ T}$. The insert schematically shows the splitting energy levels of Mn dimer in the magnetic field. (d) Field dependence of the step energy extracted from (b) (black dots). The red line is the linear fit of the step energy versus B , using $\delta E = g\mu_B B$ (corresponding to the lowest spin excitation of Mn). The fit yields a g -factor of 1.98 and a zero-field splitting energy of $0.086 \pm 0.025 \text{ meV}$. Gray dashed lines are high-order spin excitations calculated from the SH approach.

symmetric steps with respect to Fermi level (E_F), and the energy of these steps increases monotonically with B (note that the superconductivity of Pb film and Nb tip are both completely suppressed at these fields). This is a hallmark of IETS caused by spin excitations of Mn under a Zeeman field.^{24–26} Figure 1(d) shows a linear fit of the excitation energy (derived from the position of the step edges in Figure 1(b)) versus B , using $\delta E = g\mu_B B$ (μ_B is the Bohr magneton). The fit yields a Lande g -factor of 1.98 and a nonzero intercept of $0.086 \pm 0.025 \text{ meV}$ at $B = 0$. The finite intercept indicates that the Mn atom has a small magnetic anisotropy, which can be described by the spin Hamiltonian approach detailed below.

Via atom manipulation, we can construct a Mn dimer though moving the atoms (insert of Figure 1(a)). The tunneling spectrum on a dimer with interatomic spacing of 0.25 nm exhibits symmetric steps at $\pm 7.9 \text{ meV}$, which further split into three substeps at higher magnetic field strengths (Figure 1(c)). This indicates that the two Mn atoms are antiferromagnetically coupled. The split steps come from the excitation of the spin-singlet ($S = 0$) ground state to a spin-triplet ($S = 1$) state. These results are consistent with previous studies of Mn atoms on different decoupling layers^{10,24} and prove that PbO film is effective as a decoupling layer for spin excitation studies.

4,4'-Biphenyldicarbonitrile (BPCN) molecules were introduced to the PbO surface at a temperature below 50 K to form well-isolated single molecules. A BPCN molecule has two benzene rings and two carbonitrile ($-\text{CN}$) groups (Figure 2(a)), and it was visualized as a rod-shaped protrusion (length $\approx 1.71 \text{ nm}$) in the STM topography (Figure 2(b)). Using tip manipulation, we were able to move the BPCN molecule toward one of the Mn atoms. We found that when one end of the molecule (the carbonitrile group) touches a Mn atom (Figure 2(c)), the apparent height of the latter dramatically decreased to 0.12 nm. Meanwhile the BPCN molecule could not be moved away but only rotated around the anchoring Mn atom. This indicates a chemical bond was formed between carbonitrile group and Mn atom.^{30–32} A Mn complex with only one carbonitrile-coordinated ligand was constructed.

Figure 2(d, e) shows the tunneling spectra of a Mn complex (measured at the position of Mn atom) under various magnetic fields. They are substantially different from that of an individual Mn atom. At the low field strength of 1.5 T, IETS steps with an energy of 0.44 meV are observed, which is significantly larger than the Zeeman energy (0.29 meV) of single Mn atoms for the same field strength. It is noticeable that the step position varies nonmonotonically with magnetic field. In particular, at $B = 5 \text{ T}$, the spectrum shows evidence of double steps (marked by arrows in Figure 2(e)), which can be ascribed to two different spin excitations as shown below. Upon setting the field to zero, the spectra at the location of the Mn complex was dramatically changed. Under zero magnetic field, both the Pb substrate and Nb tip are superconducting. The spectrum measured on bare PbO shows sharp coherence peaks at the energy of $\pm(\Delta_{\text{tip}} + \Delta_{\text{Pb}})$ (Figure 2(d), in which Δ_{tip} and Δ_{Pb} are the energy gaps of the tip and Pb substrate).¹¹ Meanwhile, the spectrum of the Mn complex shows two symmetric small peaks outside of the coherence peak (Figure 2(d)). These small peaks actually originate from IETS signals detected by the superconducting tip. Because the tunneling conductance (dI/dV) is proportional to the convolution of the density of states (DOS) of both tip and sample, and because the DOS is strongly peaked at the superconducting gap edge of

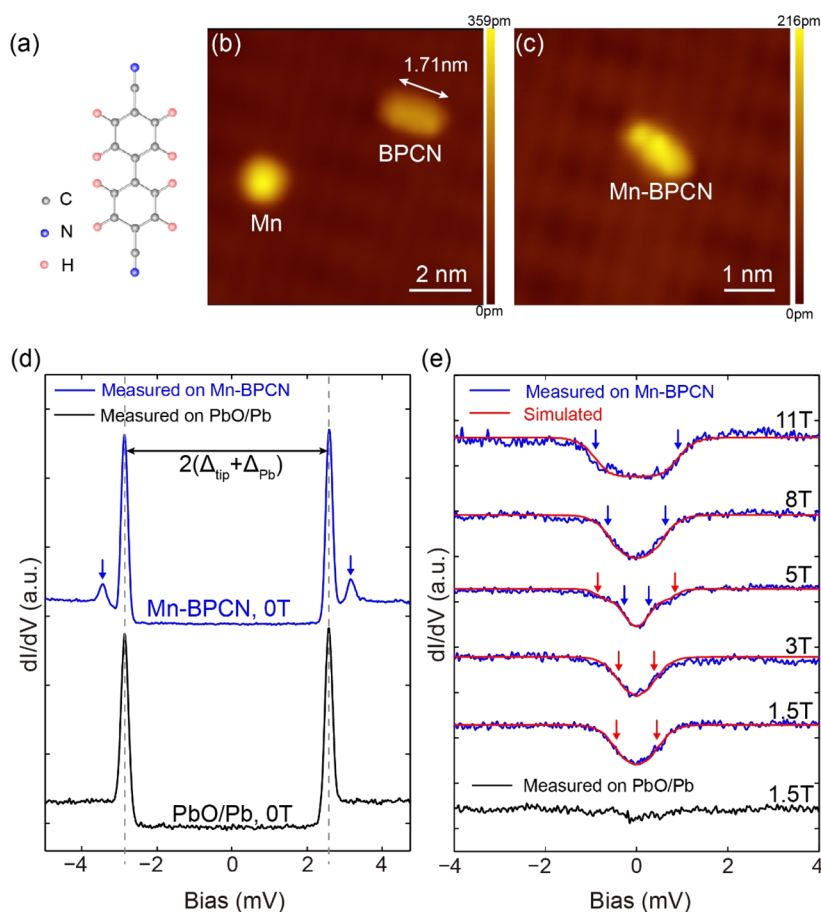


Figure 2. Mn complex and its tunneling spectra. (a) The chemical structure of 4,4'-biphenyldicarbonitrile (BPCN) molecule. (b, c) STM images of one Mn atom and one BPCN molecule before bonding (b) ($8.9 \times 8.9 \text{ nm}^2$, $V = 0.5 \text{ V}$, $I = 0.1 \text{ nA}$) and after bonding (c) ($5.5 \times 5.5 \text{ nm}^2$, $V = 0.5 \text{ V}$, $I = 0.1 \text{ nA}$). (d) dI/dV spectra on Mn complex taken by the superconducting tip at zero field (blue curve, the zero-field splitting peaks were indicated by blue arrows) and on bare PbO (black curve) for comparison. Gray dashed lines indicate the sharp coherence peaks at the energy of $\pm(\Delta_{\text{tip}} + \Delta_{\text{pb}})$. Tunneling junction: $V = 10 \text{ mV}$, $I = 0.2 \text{ nA}$. Bias modulation: $50 \mu\text{V}$, 991 Hz . $T = 0.4 \text{ K}$. (e) dI/dV spectra of the Mn complex in magnetic field (blue curves). The tunneling junction is the same as in (b). All the curves are offset vertically for clarity. Red curves are simulated spectra with an effective temperature of 1.5 K and considering the excitation intensity given by eq 2 (see text). Blue and red arrows indicate the IETS steps which come from the first and second excited states, respectively. dI/dV spectra on bare PbO at $B = 1.5 \text{ T}$ is for comparison.

the tip, the IETS steps transformed into peaks in dI/dV spectra. Therefore, the Mn complex has a spin excitation at zero field, i.e., the so-called zero-field splitting (ZFS), which is the hallmark of magnetic anisotropy. The zero-field splitting energy can be directly measured as the energy difference between a small peak and its neighboring coherence peak, which is 0.58 meV here. Similar results were reproduced on more than three different complexes. Since peaks in the dI/dV spectra give much better resolution than the steps, the superconducting tip shows its advantage in identifying the IETS feature at zero magnetic field.

To understand the spin excitation process, we introduced a spin Hamiltonian (SH) approach which usually describes the magnetic system in anisotropic environment.²⁴ The second-order SH in a magnetic field is written as

$$\hat{H} = g\mu_B \hat{B}\hat{S} + D\hat{S}_z^2 + E(\hat{S}_x^2 - \hat{S}_y^2) \quad (1)$$

The first term is the Zeeman splitting while the second and third terms phenomenologically describe the strengths of the axial and transverse magnetic anisotropies, respectively. $\hat{S} = (\hat{S}_x, \hat{S}_y, \hat{S}_z)$ is the spin operator. Diagonalizing eq 1 requires the net spin value of the Mn complex and the angle between \mathbf{B} and

\hat{S}_z . Because carbonitrile is a kind of moderate-strength field ligand,^{24,25} the Mn atom in the complex was expected to maintain its free atom spin ($S = 5/2$). We found that reasonable fitting can only be obtained by choosing \hat{S}_z perpendicular to the magnetic field. The best fit yields $D = -0.14 \pm 0.01 \text{ meV}$, $E = 0.01 \pm 0.01 \text{ meV}$, and $g = 1.97 \pm 0.02$. Calculated spin excitations and experimental IETS step energies are plotted in Figure 3(a), where the steps originated from two types of spin excitations. The eigenenergies of eq 1 from the best fit are shown in Figure 3(b). A negative D means the Mn complex has an easy-axis magnetic anisotropy, which lifts the spin sextuplet degenerate ground state into three Kramers doublets. The observed zero-field splitting is the excitation from the first doublet ($m = \pm 5/2$) to the second doublet ($m = \pm 3/2$). A magnetic field perpendicular to the main anisotropy axis lifts the doublets by the Zeeman effect and mixes spin states of different magnetic quantum number m . However, when the Zeeman energy is not comparable to the zero-field splitting energy, the splitting of the first (ground) doublet with high $|m|$ is weak, which is the reason that we did not observe the first excitation at lower magnetic field strengths.

In IETS, the intensity of spin excitations (represent as the relative height of IETS steps) is related to the spin selection

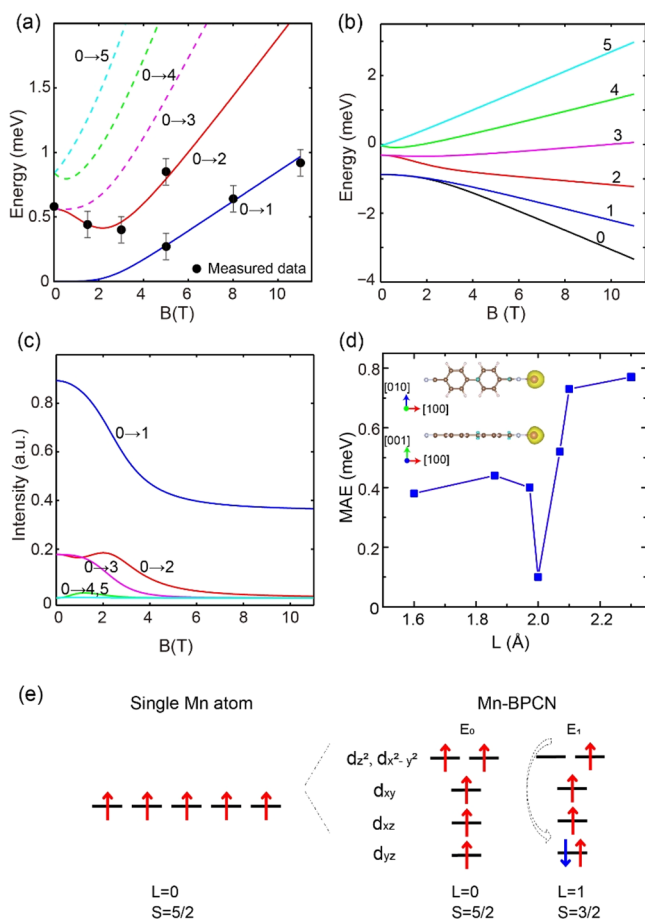


Figure 3. Spin excitations of the Mn complex. (a) Black dots: Energies of the first and second excited states extracted from the IET steps in Figure 2(e) and zero-field splitting in Figure 2(d). Solid lines: Calculated spin excitation energies by eq 1 with the magnetic field perpendicular to the \hat{S}_z direction (using $D = -0.139$ meV, $E = 0.001$ meV, and $g = 1.97$). The marks next to curves indicate the excitation level. (b) The eigenvalues of eq 1 with the same anisotropy parameter of (a), where numbers mark different states. (c) Calculated relative spin excitation intensities from eq 2. (d) The magnetic anisotropy energy (blue dots) is defined as $MAE = E_{[001]} - E_{[010]}$ with seven different Mn–N bond lengths around ~ 2.0 Å. The inset shows the spatial distribution of the net spin for the Mn-BPCN complex with the isosurface of 0.015 $e^-/\text{\AA}^3$, corresponding to the yellow color surrounding the Mn atom (the upper one is the top view and the lower one is the side view). (e) Energy level diagram of a single Mn atom and Mn-BPCN complex. E_0 and E_1 represent the electronic ground and first excited states of the Mn-BPCN complex.

rule^{24,26} and the exchange interaction between tunneling electron spin and atomic spin.^{33–35} The weight of observed IETS steps can be qualitatively described as^{10,33}

$$I_{i-f} = |\langle \Psi_f | \hat{S}_x | \Psi_i \rangle|^2 + |\langle \Psi_f | \hat{S}_y | \Psi_i \rangle|^2 + |\langle \Psi_f | \hat{S}_z | \Psi_i \rangle|^2 \quad (2)$$

where Ψ_f and Ψ_i are the final and initial spin states, respectively. Using the eigenvectors of eq 1, spin excitation intensities were calculated as a function of the magnetic field, as shown in Figure 3(c). The first excitation has the largest intensity and thus should be observed at $B > 4$ T (at 0.4 K, the thermal broadening is around 0.1 meV). The second and third excitations are too weak to be observed at high field. The fourth and fifth excitations have almost zero intensity and cannot be observed at all. We modeled the tunneling spectra in

Figure 2(e), using the calculated excitation intensities and with considering thermal and equipment broadening. The fitted curves (Figure 2(e)) show good agreement with the experimental spectra.

As previously mentioned, single Mn atoms on PbO only show a small zero-field splitting energy of 0.086 meV. By fitting the IETS steps of single atoms on PbO in Figure 1 with eq 1 using $S = 5/2$, we obtained $D = -0.022$ meV, $g = 1.98$, and the z -axis parallel to B (out-of-plane). This suggests that the PbO substrate was weakly coupled to Mn and only induced small easy-axis (out-of-plane) anisotropy, which is similar to the case of Mn atoms adsorbed on thin CuN or Al_2O_3 .^{10,24} However, when the Mn atom is chemically bonded to a carbonitrile group, the zero-field splitting energy was substantially increased and the main axis was reoriented to the in-plane direction. The enhanced anisotropy should be due to the strong anisotropic ligand field given by the single carbonitrile ligand, which is further supported by the density functional theory (DFT) calculations below. Since the BPCN molecule can be rotated around the Mn atom, we also provide a method to control the direction of the anisotropy axis (or magnetization) at the level of a single molecule.

To gain microscopic understanding on the origin of magnetic anisotropy, we carried out the DFT calculations on the Mn-BPCN complex. Considering that the PbO substrate has a negligible role in affecting the magnetic properties of Mn atoms, we neglect in our calculations the interactions between the magnetic complex and the substrate. The optimized geometry is a linear structure with a one-fold coordinated BPCN. The axial line of the ligand is defined as the [100] direction, which is illustrated in the inset of Figure 3(d). The bond length of Mn–N in the relaxed structure (shown in Figure S2) is 1.973 Å. This short Mn–N distance, which was equivalent to the sum of the covalent radii of Mn and N atoms (1.19 and 0.71 Å, respectively), implies that a covalent bond was formed between the Mn and N atom. Electron localization function (ELF) analysis (shown in Figure S3(a)) in the (001) plane of BPCN–Mn complex, which was used to describe the localization of electronic groups and the chemical bonds, shows that the high ELF (around 0.90) region between the N and Mn atom deviates from the center and is inclined to the N atom, suggesting a ligand bond. In addition, charge density difference analysis (shown in Figure S3(b)) between the BPCN molecule and the Mn atom indicates that the electron cloud in the Mn–N bond interstice is dominated by the p electron of the N atom and the d orbital of the Mn atom, verifying the ligand property of the Mn–N chemical bond. In order to quantitatively investigate the magnetic anisotropy of low coordinated Mn-BPCN, we calculated the system's energy when the magnetic moment is confined in three different axes' directions with seven different Mn–N bond lengths around ~ 2.0 Å, and spin–orbit coupling is considered. The magnetic anisotropy energy (defined as $MAE = E_{[001]} - E_{[010]}$) in Figure 3(d) shows a lower energy of the [010] axis than that of out-of-plane [001], indicating an easy-axis magnetic anisotropy along the [010] direction in the plane, which is consistent with the fitting results from experimental data.

Magnetic anisotropy originates from a crystal-field (CF) effect combined with spin–orbit interaction (SOI). Transition-metal atoms in low-symmetry environments usually show large magnetic anisotropies.^{9,10} Nevertheless, the Mn atom (and Mn^{II} ion) with d^5 configuration is unconventional because its free atom ground state is an orbital singlet (${}^6A_{1g}$). This $L = 0$

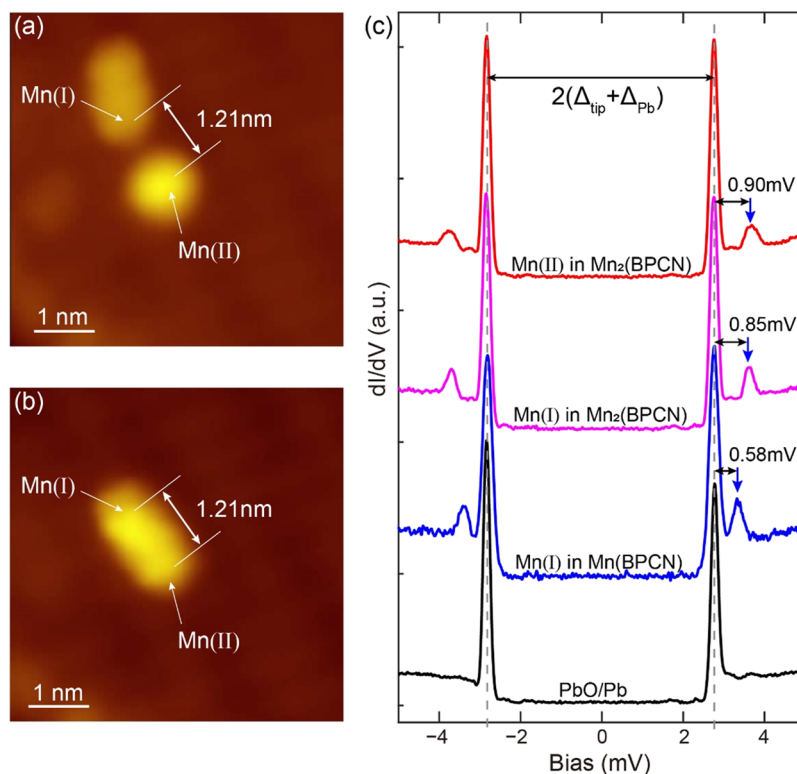


Figure 4. Demonstration of constructing a compressed $\text{Mn}_2(\text{BPCN})$. (a) STM image of a free-standing $\text{Mn}(\text{BPCN})$ complex (top) and another single Mn atom (center). Arrows indicate the location of Mn atoms ($5.5 \times 5.5 \text{ nm}^2$, $V = 1.0 \text{ V}$, $I = 0.1 \text{ nA}$). (b) Rotation of the BPCN molecule to the Mn(II) atom and their bonding, where arrows indicate the position of Mn atoms in the complex. (c) dI/dV spectra of Mn atoms in $\text{Mn}(\text{BPCN})$ (blue curve) and compressed $\text{Mn}_2(\text{BPCN})$ complex (magenta and red curves) taken by the superconducting tip at zero field, where the zero-field splitting peaks are indicated by blue arrows. Note that the zero-field splitting peaks move toward to high energy after compressed bonding formed. The dI/dV spectra on bare PbO (black curve) are for comparison. Gray dashed lines indicate the sharp coherence peaks at the energy of $\pm(\Delta_{\text{tip}} + \Delta_{\text{Pb}})$. Tunneling junction: $V = 10 \text{ mV}$, $I = 0.2 \text{ nA}$. Bias modulation: $50 \mu\text{V}$, 991 Hz . $T = 0.4 \text{ K}$.

ground state will not be directly split by the crystal (ligand) field and SOI, resulting in a small easy-axis anisotropy of single Mn atoms. Thus, the magnetic anisotropy of the Mn complex is thought to arise from the mixing of spin excited states and ground states through high-order perturbation^{36,37} that is usually weak.^{38,39}

By further analyzing the net spin in the spatial distribution (see the inset in Figure 3(d)) for the Mn-BPCN complex, we found that the net spin is mainly localized on the Mn atom and the spin moment is preserved to be the free form of $5 \mu_B$. The projected density of states (PDOS) of d-orbital for Mn-BPCN complex (shown in Figure S4) reveals that the molecular ligand field lifts the degenerate d orbitals of Mn atom and leads to a change in the d orbital alignment. The actual orbital orders an energy diagram where $d_{x^2-y^2}$ and d_z^2 orbitals remain degenerate and all the orbitals are singly occupied by electrons with the same spin direction, preserving high-spin $S = 5/2$ ground state E_0 (Figure 3(e)). In this case, the quenched orbital angular momentum ($L = 0$) suppresses SOI ($\hat{H}_{\text{SOC}} = \lambda \hat{L} \times \hat{S}$), which was required to develop the magnetic anisotropy. Fortunately, the weak ligand field splits the d orbitals with a small total energy difference between the ground state and excited state ($E_1 - E_0$), as depicted in Figure 3(e). Hence, the mixing between excited state in ^4P spin configuration ($S = 3/2$, $L = 1$) and the ground state in the ^6S term ($S = 5/2$, $L = 0$) facilitates the spin-orbital coupling to enhance the magnetic anisotropy. In other words, the low-lying excited states could

couple with the ground state, leading to a large zero-field splitting of the Mn complex.

This magnetic anisotropy arises from the carbonitrile ligand. Its value is expected to depend on the coupling of the ligand field with Mn, which varies with the distance between Mn and carbonitrile group. To confirm this, we constructed a Mn_2BPCN complex (Figure 4 (a) and (b) show the manipulation process, where each carbonitrile group of BPCN is bonded to one Mn atom), in which the distance between two Mn atoms (1.21 nm, see Figure 4(b)) is shorter than the length of free BPCN (1.71 nm, see Figure 2(b)). Thus, the BPCN molecule was considered to be compressed (Mn atoms do not move during the manipulation), and the distance between Mn and carbonitrile are supposed to be smaller than the free-standing case. Figure 4(c) shows the spectrum taken on Mn_2BPCN at zero field. As expected, the zero-field splitting of the two Mn atoms in the compressed structure increased to 0.85 and 0.90 meV, respectively. These values are larger than the anisotropy values observed in common Mn molecular compounds.

The controllably constructed Mn complex on PbO can be considered as a prototype of molecular magnets.²⁵ The PbO insulating layer is essential here because it allows us to observe the intrinsic properties of magnetic structures. We demonstrated a bottom-up way to tune the ligand field at the single molecule level and study the induced magnetic behavior. In principle, a 2D molecular magnetic network could be built using this approach. Further studies could involve different

magnetic atoms with different types and numbers of ligands. This research result is of great importance for designing molecular magnets or spin nanostructures with desired properties.

■ ASSOCIATED CONTENT

Supporting Information

The Supporting Information is available free of charge at <https://pubs.acs.org/doi/10.1021/acs.nanolett.1c00545>.

Methods for first-principles calculations; large-scale STM images of PbO/Pb/Si(111) film; configuration and the calculated energy of the BPCN-Mn complex; electron localization function and charge density difference analysis of the BPCN-Mn complex; calculated spin-polarized projected density of states (PDOS) of d-orbitals of the Mn atom in BPCN-Mn; and the total energy of the BPCN-Mn complex with different magnetization directions for various CN-Mn bond length (PDF)

■ AUTHOR INFORMATION

Corresponding Author

Qi-kun Xue – Department of Physics, Tsinghua University, Beijing 100084, China; Email: qkxue@mail.tsinghua.edu.cn

Authors

Peng Cheng – Institute of Physics, Chinese Academy of Sciences, Beijing 100080, China; School of Physics, University of Chinese Academy of Sciences, Beijing 100049, China; orcid.org/0000-0001-5963-1390

Longjuan Kong – Institute of Physics, Chinese Academy of Sciences, Beijing 100080, China

Tong Zhang – State Key Laboratory of Surface Physics, Department of Physics, and Advanced Materials Laboratory, Fudan University, Shanghai 200438, China; Shanghai Research Center for Quantum Sciences, Shanghai 201315, China

Hang Liu – Institute of Physics, Chinese Academy of Sciences, Beijing 100080, China

Huixia Fu – Institute of Physics, Chinese Academy of Sciences, Beijing 100080, China

Lan Chen – Institute of Physics, Chinese Academy of Sciences, Beijing 100080, China; School of Physics, University of Chinese Academy of Sciences, Beijing 100049, China; orcid.org/0000-0003-4426-9944

Kehui Wu – Institute of Physics, Chinese Academy of Sciences, Beijing 100080, China; School of Physics, University of Chinese Academy of Sciences, Beijing 100049, China; orcid.org/0000-0002-7698-5673

Xi Chen – Department of Physics, Tsinghua University, Beijing 100084, China

Sheng Meng – Institute of Physics, Chinese Academy of Sciences, Beijing 100080, China; orcid.org/0000-0002-1553-1432

Complete contact information is available at: <https://pubs.acs.org/doi/10.1021/acs.nanolett.1c00545>

Author Contributions

#P.C., L.K., and T.Z. contributed equally to this work.

Notes

The authors declare no competing financial interest.

■ ACKNOWLEDGMENTS

This work is supported by the National Key R&D Program of MOST, China (2018YFE0202700, 2017YFA0303004), the National Natural Science Foundation of China (11421404, 11961160717, 11761141013, 11674368), the Shanghai Municipal Science and Technology Major Project (2019SHZDZX01), the Beijing Natural Science Foundation (Z180007), and the Strategic Priority Research Program of the Chinese Academy of Sciences (XDB30000000).

■ REFERENCES

- (1) Gatteschi, D.; Sessoli, R.; Villain, J. *Molecular Nanomagnets*; Oxford University Press: Oxford, 2006.
- (2) Kahn, O. *Molecular Magnetism*; Wiley-VCH: New York, 1993.
- (3) Leuenberger, M. N.; Loss, D. Quantum Computing in Molecular Magnets. *Nature* **2001**, *410*, 789–793.
- (4) Wolf, S. A.; Awschalom, D. D.; Buhrman, R. A.; Daughton, J. M.; von Molnár, S.; Roukes, M. L.; Chtchelkanova, A. Y.; Treger, D. M. Spintronics: A Spin-Based Electronics Vision for the Future. *Science* **2001**, *294*, 1488–1495.
- (5) Khajetoorians, A. A.; Heinrich, A. J. Toward Single-Atom Memory. *Science* **2016**, *352*, 296–297.
- (6) Loth, S.; Etzkorn, M.; Lutz, C. P.; Eigler, D. M.; Heinrich, A. J. Measurement of Fast Electron Spin Relaxation Times with Atomic Resolution. *Science* **2010**, *329*, 1628–1630.
- (7) Rau, I. G.; Baumann, S.; Rusponi, S.; Donati, F.; Stepanow, S.; Gragnaniello, L.; Dreiser, J.; Piamonteze, C.; Nolting, F.; Gangopadhyay, S.; Albertini, O. R.; Macfarlane, R. M.; Lutz, C. P.; Jones, B. A.; Gambardella, P.; Heinrich, A. J.; Brune, H. Reaching the Magnetic Anisotropy Limit of a 3d Metal Atom. *Science* **2014**, *344*, 988–992.
- (8) Paul, W.; Yang, K.; Baumann, S.; Romming, N.; Choi, T.; Lutz, C. P.; Heinrich, A. J. Control of the Millisecond Spin Lifetime of an Electrically Probed Atom. *Nat. Phys.* **2017**, *13*, 403–407.
- (9) Gambardella, P.; Rusponi, S.; Veronese, M.; Dhesi, S. S.; Grazioli, C.; Dallmeyer, A.; Cabria, I.; Zeller, R.; Dederichs, P. H.; Kern, K.; Carbone, C.; Brune, H. Giant Magnetic Anisotropy of Single Cobalt Atoms and Nanoparticles. *Science* **2003**, *300*, 1130–1133.
- (10) Hirjibehedin, C. F.; Lin, C.-Y.; Otte, A. F.; Ternes, M.; Lutz, C. P.; Jones, B. A.; Heinrich, A. J. Large Magnetic Anisotropy of a Single Atomic Spin Embedded in a Surface Molecular Network. *Science* **2007**, *317*, 1199–1203.
- (11) Otte, A. F.; Ternes, M.; von Bergmann, K.; Loth, S.; Brune, H.; Lutz, C. P.; Hirjibehedin, C. F.; Heinrich, A. J. The role of magnetic anisotropy in the Kondo effect. *Nat. Phys.* **2008**, *4*, 847–850.
- (12) Khajetoorians, A. A.; Chilian, B.; Wiebe, J.; Schuwalow, S.; Lechermann, F.; Wiesendanger, R. Detecting excitation and magnetization of individual dopants in a semiconductor. *Nature* **2010**, *467*, 1084–1087.
- (13) Parks, J. J.; Champagne, A. R.; Costi, T. A.; Shum, W. W.; Pasupathy, A. N.; Neuscammann, E.; Flores-Torres, S.; Cornaglia, P. S.; Aligia, A. A.; Balseiro, C. A.; Chan, G. K.-L.; Abruña, H. D.; Ralph, D. C. Mechanical Control of Spin States in Spin-1 Molecules and the Underscreened Kondo Effect. *Science* **2010**, *328*, 1370–1373.
- (14) Bryant, B.; Spinelli, A.; Wagenaar, J. J. T.; Gerrits, M.; Otte, A. F. Local control of single atom magnetocrystalline anisotropy. *Phys. Rev. Lett.* **2013**, *111*, 127203.
- (15) Miyamachi, T.; Schuh, T.; Märkl, T.; Bresch, C.; Balashov, T.; Stöhr, A.; Karlewski, C.; André, S.; Marthaler, M.; Hoffmann, M.; Geilhufe, M.; Ostanin, S.; Hergert, W.; Mertig, I.; Schön, F.; Ernst, A.; Wulfhkel, W. Stabilizing the magnetic moment of single holmium atoms by symmetry. *Nature* **2013**, *503*, 242–246.
- (16) Gambardella, P.; Stepanow, S.; Dmitriev, A.; Honolka, J.; deGroot, F. M. F.; Lingenfelder, M.; Gupta, S. S.; Sarma, D. D.; Bencok, P.; Stanescu, S.; Clair, S.; Pons, S.; Lin, N.; Seitsonen, A. P.; Brune, H.; Barth, J. V.; Kern, K. Supramolecular control of the

magnetic anisotropy in two-dimensional high-spin Fe arrays at a metal interface. *Nat. Mater.* **2009**, *8*, 189–193.

(17) Tsukahara, N.; Noto, K.; Ohara, M.; Shiraki, S.; Takagi, N.; Takata, Y.; Miyawaki, J.; Taguchi, M.; Chainani, A.; Shin, S.; Kawai, M. Adsorption-Induced Switching of Magnetic Anisotropy in a Single Iron(II) Phthalocyanine Molecule on an Oxidized Cu(110) Surface. *Phys. Rev. Lett.* **2009**, *102*, 167203.

(18) Heinrich, B. W.; Ahmadi, G.; Müller, V. L.; Braun, L.; Pascual, J. I.; Franke, K. J. Change of the Magnetic Coupling of a Metal–Organic Complex with the Substrate by a Stepwise Ligand Reaction. *Nano Lett.* **2013**, *13*, 4840–4843.

(19) Heinrich, B. W.; Braun, L.; Pascual, J. I.; Franke, K. J. Protection of Excited Spin States by a Superconducting Energy Gap. *Nat. Phys.* **2013**, *9*, 765–768.

(20) Heinrich, B. W.; Braun, L.; Pascual, J. I.; Franke, K. J. Tuning the Magnetic Anisotropy of Single Molecules. *Nano Lett.* **2015**, *15*, 4024–4028.

(21) Stoll, P.; Bernien, M.; Rolf, D.; Nickel, F.; Xu, Q.; Hartmann, C.; Umbach, T. R.; Kopprasch, J.; Ladenthin, J. N.; Schierle, E.; Weschke, E.; Czekelius, C.; Kuch, W.; Franke, K. J. Magnetic Anisotropy in Surface-Supported Single-Ion Lanthanide Complexes. *Phys. Rev. B: Condens. Matter Mater. Phys.* **2016**, *94*, 224426.

(22) Ormaza, M.; Bachellier, N.; Faraggi, M. N.; Verlhac, B.; Abufager, P.; Ohresser, P.; Joly, L.; Romeo, M.; Scheurer, F.; Bocquet, M.-L.; Lorente, N.; Limot, L. Efficient Spin-Flip Excitation of a Nickelocene Molecule. *Nano Lett.* **2017**, *17*, 1877–1882.

(23) Liu, B.; Fu, H. X.; Guan, J. Q.; Shao, B.; Meng, S.; Guo, J. D.; Wang, W. H. An Iron-Porphyrin Complex with Large Easy-Axis Magnetic Anisotropy on Metal Substrate. *ACS Nano* **2017**, *11*, 11402–11408.

(24) Heinrich, A. J.; Gupta, J. A.; Lutz, C. P.; Eigler, D. M. Single-Atom Spin-Flip Spectroscopy. *Science* **2004**, *306*, 466–469.

(25) Hirjibehedin, C. F.; Lutz, C. P.; Heinrich, A. J. Spin Coupling in Engineered Atomic Structures. *Science* **2006**, *312*, 1021–1024.

(26) Chen, X.; Fu, Y. S.; Ji, S. H.; Zhang, T.; Cheng, P.; Ma, X. C.; Zou, X. L.; Duan, W. H.; Jia, J. F.; Xue, Q. K. Probing superexchange interaction in molecular magnets by spin-flip spectroscopy and microscopy. *Phys. Rev. Lett.* **2008**, *101*, 197208.

(27) Ji, S. H.; Zhang, T.; Fu, Y. S.; Chen, X.; Ma, X. C.; Li, J.; Duan, W. H.; Jia, J. F.; Xue, Q. K. High-Resolution Scanning Tunneling Spectroscopy of Magnetic Impurity Induced Bound States in the Superconducting Gap of Pb Thin Films. *Phys. Rev. Lett.* **2008**, *100*, 226801.

(28) Ma, X. C.; Jiang, P.; Qi, Y.; Jia, J. F.; Yang, Y.; Duan, W. H.; Li, W. X.; Bao, X. H.; Zhang, S. B.; Xue, Q. K. Experimental observation of quantum oscillation of surface chemical reactivities. *Proc. Natl. Acad. Sci. U. S. A.* **2007**, *104*, 9204–9208.

(29) Fu, Y. S.; Ji, S. H.; Zhang, T.; Chen, X.; Ma, X. C.; Jia, J. F.; Xue, Q. K. Ultrathin lead oxide film on Pb(111) and its application in single spin detection. *Appl. Phys. Lett.* **2009**, *95*, 063107.

(30) Repp, J.; Meyer, G.; Paavilainen, S.; Olsson, F.; Persson, M. Imaging Bond Formation between a Gold Atom and Pentacene on an Insulating. *Science* **2006**, *312*, 1196–1199.

(31) Wahl, P.; Diekhoner, L.; Wittich, G.; Vitali, L.; Schneider, M. A.; Kern, K. Kondo Effect of Molecular Complexes at Surfaces: Ligand Control of the Local Spin Coupling. *Phys. Rev. Lett.* **2005**, *95*, 166601.

(32) Wegner, D.; Yamachika, R.; Zhang, X. W.; Wang, Y. Y.; Baruah, T.; Pederson, M. R.; Bartlett, B. M.; Long, J. R.; Crommie, M. F. Tuning Molecule-Mediated Spin Coupling in Bottom-Up-Fabricated Vanadium-Tetracyanoethylene Nanostructures. *Phys. Rev. Lett.* **2009**, *103*, 087205.

(33) Fernandez-Rossier, J. Theory of Single-Spin Inelastic Tunneling Spectroscopy. *Phys. Rev. Lett.* **2009**, *102*, 256802.

(34) Fransson, J. Spin Inelastic Electron Tunneling Spectroscopy on Local Spin Adsorbed on Surface. *Nano Lett.* **2009**, *9*, 2414–2417.

(35) Lorente, N.; Gauyacq, J.-P. Efficient Spin Transitions in Inelastic Electron Tunneling Spectroscopy. *Phys. Rev. Lett.* **2009**, *103*, 176601.

(36) Blume, M.; Orbach, R. Spin-Lattice Relaxation of S-State Ions: Mn^{2+} in a Cubic Environment. *Phys. Rev.* **1962**, *127*, 1587.

(37) Yu, W. L.; Zhao, M. G. Spin-Hamiltonian parameters of f^6 state ions. *Phys. Rev. B: Condens. Matter Mater. Phys.* **1988**, *37*, 9254.

(38) Boca, R. Zero-field splitting in metal complexes. *Coord. Chem. Rev.* **2004**, *248*, 757–815.

(39) Krzystek, J.; Ozarowski, A.; Telser, J. Multi-frequency, high-field EPR as a powerful tool to accurately determine zero-field splitting in high-spin transition metal coordination complexes. *Coord. Chem. Rev.* **2006**, *250*, 2308–2324.